Interaction effects on galaxy pairs with Gemini/GMOS – II: oxygen abundance gradients

D. A. Rosa,[1][*] O. L. Dors Jr,[1] A. C. Krabbe,[1] G. F. Hägele,[2,3] M. V. Cardaci,[2,3]
M. G. Pastoriza,[4] I. Rodrigues[1] and C. Winge[5]

[1]*Universidade do Vale do Paraíba, Av. Shishima Hifumi, 2911, Cep 12244-000, São José dos Campos, SP, Brazil*
[2]*Instituto de Astrofísica de La Plata (CONICET La Plata–UNLP), Argentina*
[3]*Facultad de Ciencias Astronómicas y Geofísicas, Universidad Nacional de La Plata, Paseo del Bosque s/n, 1900 La Plata, Argentina*
[4]*Instituto de Física, Universidade Federal do Rio Grande do Sul, Av. Bento Gonçalves, 9500, Cep 91359-050, Porto Alegre, RS, Brazil*
[5]*Gemini Observatory, c/o AURA Inc., Casilla 603, La Serena, Chile*

ABSTRACT

In this paper, we derive oxygen abundance gradients from H II regions located in 11 galaxies in eight systems of close pairs. Long-slit spectra in the range 4400–7300 Å were obtained with the Gemini Multi-Object Spectrograph at Gemini South (GMOS-S). Spatial profiles of oxygen abundance in the gaseous phase along galaxy discs were obtained using calibrations based on strong emission lines ($N2$ and $O3N2$). We found oxygen gradients to be significantly flatter for all the studied galaxies than those in typical isolated spiral galaxies. Four objects in our sample, AM 1219A, AM 1256B, AM 2030A and AM 2030B, show a clear break in the oxygen abundance at galactocentric radius R/R_{25} between 0.2 and 0.5. For AM 1219A and AM 1256B, we found negative slopes for the inner gradients, and for AM 2030B, we found a positive slope. All three cases show a flatter behaviour to the outskirts of the galaxies. For AM 2030A, we found a positive slope for the outer gradient, while the inner gradient is almost compatible with a flat behaviour. We found a decrease of star formation efficiency in the zone that corresponds to the oxygen abundance gradient break for AM 1219A and AM 2030B. For the former, a minimum in the estimated metallicities was found very close to the break zone, which could be associated with a corotation radius. However, AM 1256B and AM 2030A, present a star formation rate maximum but not an extreme oxygen abundance value. All four interacting systems that show oxygen gradient breaks have extreme SFR values located very close to break zones. The H II regions located in close pairs of galaxies follow the same relation between the ionization parameter and the oxygen abundance as those regions in isolated galaxies.

Key words: techniques: imaging spectroscopy – ISM: abundances – galaxies: abundances – galaxies: interactions.

1 INTRODUCTION

The study of the chemical evolution of galaxies, both isolated galaxies and interacting galaxies, plays an important role in the understanding of the formation of these objects, the stellar formation history and the evolution of the Universe.

In general, for almost all disc isolated galaxies, a negative oxygen gradient is derived, such as our Galaxy (Vílchez & Esteban 1996; Andrievsky et al. 2002, 2004; Luck et al. 2003; Costa, Uchida & Maciel 2004; Bragaglia et al. 2008; Maciel & Costa 2009; Magrini et al. 2009; Pedicelli et al. 2009; Esteban et al. 2013; Lemasle

et al. 2013; Yong, Carney & Friel 2014). This negative gradient is naturally explained by models that assume the growth in the inside-out scenario of galaxies (Portinari & Chiosi 1999; Boissier & Prantzos 2000; Mólla & Díaz 2005), where galaxies begin to form their inner regions before the outer regions, as confirmed by stellar population studies of spiral galaxies (Bell & Jong 2000; MacArthur et al. 2004; Pohlen & Trujillo 2006; Muñoz-Mateos et al. 2007) and by very deep photometric studies of galaxies at high redshifts (Trujillo et al. 2004; Barden et al. 2005).

The oxygen gradients can be flattened or modified by the presence of gas flows along the galactic disc. Basically, these gas flows could arise as a result of two mechanisms. In isolated galaxies, hydrodynamical simulations predict that the bars might produce a falling of gas into the central regions (Athanassoula 1992;

[*]E-mail: deiserosa@univap.br

Friedli et al. 1994; Perez et al. 2006, 2011), as confirmed by observational studies (Martin & Roy 1994; Zaritsky, Kennicutt & Huchra 1994). The second mechanism occurs in interacting galaxies or close pairs, where interaction-induced gas flows from the outer parts to the centre of each component (Toomre & Toomre 1972; Dalcanton 2007) seem to modify the metallicity in galactic discs. Therefore, the metallicity gradients of interacting galaxies or galaxies that have had an interaction in the past are shallower (Bresolin et al. 2009a; Rupke, Kewley & Barnes 2010a; Miralles-Caballero et al. 2014; Sánchez et al. 2014) than those derived for isolated galaxies (Rupke et al. 2010a; Sánchez et al. 2012). In fact, by combining long-slit spectroscopy data for the interacting pairs AM 2306–721 and AM 2322–821 with grids of photoionization models, Krabbe et al. (2008, 2011) found shallower metallicity gradients than those in isolated spiral galaxies. However, recently, there have been two works in which the first systematic investigations into metallicity gradients in interacting galaxies have been conducted. First, Kewley et al. (2010) have determined the metallicity gradients for eight galaxies in close pairs and have found them to be shallower than gradients in isolated spiral galaxies. Secondly, using data obtained from the Calar Alto Legacy Integral Field Area (CALIFA) survey, Sánchez et al. (2014) have found that galaxies with evidence of interactions and/or clear merging systems present significantly shallower gradients.

Furthermore, the gas motions produced by the interactions also induced star formation along the disc of the galaxies involved (Alonso et al. 2012), and this burst of star formation might be associated with a flatter metallicity gradient (Kewley et al. 2010). For example, Chien et al. (2007) determined the oxygen abundance of 12 young star clusters in the merging galaxy pair NGC 4676. They found a nearly flat oxygen distribution along the northern tail of this object, suggesting efficient gas mixing (see also Trancho et al. 2007; Bastian et al. 2009). Recently, using a large sample of galaxy pairs taken from the Sloan Digital Sky Survey Data Release 7, Scudder et al. (2012) found that galaxies in pairs show a star formation rate (SFR) about 60 per cent higher than that in non-pair galaxies (see also Barton, Geller & Kenyon 2000; Lambas et al. 2003; Nikolic, Cullen & Alexander 2004). Additional analysis of these data by Ellison et al. (2013), who investigated the effects of galaxy mergers throughout the interaction sequence, has revealed an enhancement of the average central SFR by a factor of about 3.5 in relation to the one in objects with no close companion. Ellison et al. (2013) also found a stronger deficit in the gas phase metallicity in the post-merger sample than in closest pairs (see also Bernloehr 1993; Barton et al. 2000; Bergvall, Laurikainen & Aalto 2003; Lambas et al. 2003; Di Matteo, Bournaud & Martig 2008; Mihos, Bothun & Richstone 2010; Freedman Woods et al. 2010; Patton et al. 2011; Alonso et al. 2012).

Although there have been recent efforts to improve our understanding of the effects of interactions on the chemical evolution of galaxies (Krabbe et al. 2008; Kewley et al. 2010; Krabbe et al. 2011; Bresolin, Kennicutt & Ryan-Weber 2012; Torres-Flores et al.

2014), the number of galaxies in close pairs for which the metallicity has been estimated along their galactic discs is insufficient for a statistical analysis. Our main goal in this paper is to increase the number of determinations of metallicity gradients in galaxy pairs in order to increase our knowledge of several phenomena that arise during the interactions.

In previous work (Krabbe et al. 2014, hereafter Paper I), we presented an observational study of the effect of the interactions on the electron density of H II regions located in seven systems of interacting galaxies. We found that the electron density estimates obtained in our sample are systematically higher than those derived for isolated galaxies. In the present paper, we mainly use these data to estimate the metallicity gradients along the discs of eight galaxy pairs. This paper is organized as follows. In Section 2, we summarize the observations and data reduction. In Section 3, we describe the method used to compute the metallicity of the gas phase of our sample. We present the results in Section 4, and we discuss the results in Section 5. We give our conclusions of the outcomes in Section 6.

2 OBSERVATIONAL DATA

We have selected eight close pair systems from Ferreiro & Pastoriza (2004) to study the effects of minor mergers on the gradient abundances of individual galaxies. We selected objects with a mass ratio in the range of $0.04 < M_{secondary}/M_{primary} < 0.2$, with an apparent B magnitude higher than 18, with redshift in the range $0.01 \lesssim z \lesssim 0.06$, and classified as close interacting pairs.

Long-slit spectroscopic data of the galaxy systems AM 1054–325, AM 1219–430, AM 1256–433, AM 2030–303, AM 2058–381, AM 2229–735, AM 2306–721 and AM 2322–821 were obtained with the Gemini Multi-Object Spectrograph (GMOS) attached to the 8-m Gemini South telescope. Spectra in the range 4400–7300 Å were acquired with the B600 grating, a slit width of 1 arcsec and a spectral resolution of ∼5.5 Å. Except for AM 2030–303, detailed information on the galaxy systems observed, containing most of the slit positions for each system and a complete description of the data reduction, were presented in Paper I, and are not reproduced here.

AM 2030–303 is the only object in our sample that was not included in Paper I and its main information is presented in Table 1. For the systems AM 1256–433 and AM 2058–381, one more slit position than the ones presented in Paper I is considered in the present work: position angles (PAs) 70° and 28°, respectively. It is important to note that for some systems of galaxies (e.g. AM 2306–721 and AM 2322–821; see Krabbe et al. 2008, 2011) we had spectra in the range of about 3400–7300 Å. However, in order to obtain homogeneous metallicity determination, we restricted the analysis to the same wavelength range (i.e. 4400–7300 Å). In Fig. 1, the slit positions for these three systems are shown superimposed on the GMOS-S r' acquisition image (see fig. 1 of Paper I for the slit positions of the other five objects). These data were not included in

Table 1. Morphological type, right ascension, declination, radial velocity, magnitude and cross-identifications for AM 2030–303.

ID	Morphology	α(2000)	δ(2000)	cz (km s^{-1})	m_B (mag)	Other names
AM 2030-303	SA?[a]	20^h 33^m 56^{s}3	−30°22′41″	12 323[a]	15.25[b]	ESO 463-IG 003 NED01
	G Trpl[b]	20^h 33^m 59^{s}7	−30°22′29″	12 465[a]	17.80[b]	ESO 463-IG 003 NED02
	G Trpl[b]	20^h 33^m 59^{s}7	−30°22′23″	12 474[a]	21.39[b]	ESO 463-IG 003 NED03

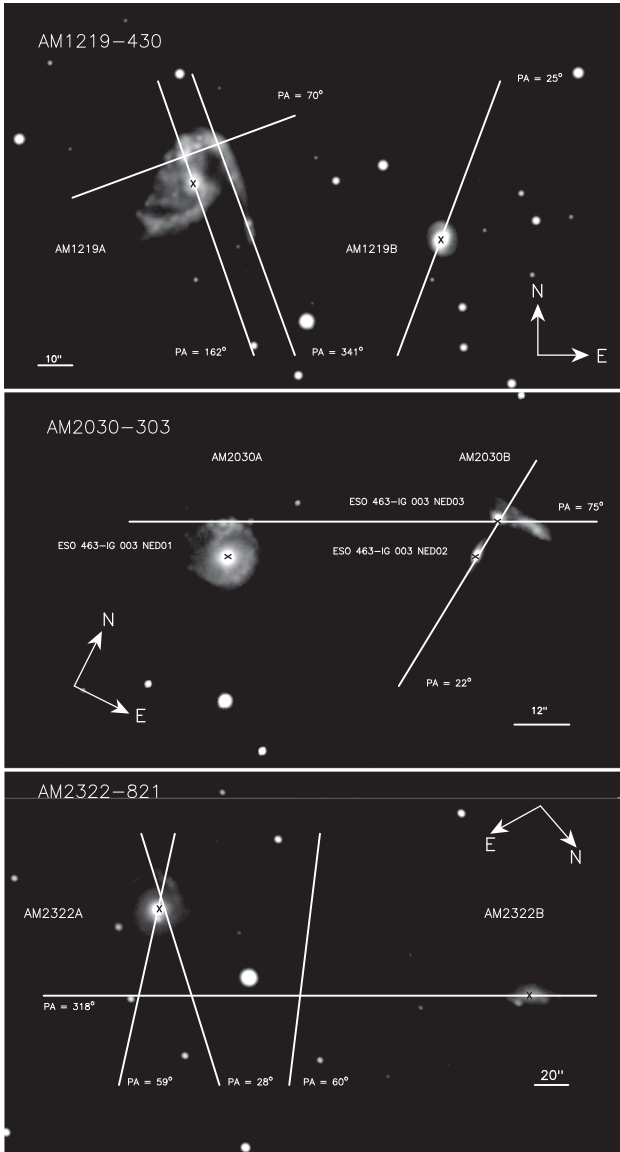[a]Donzelli & Pastoriza (1997).
[b]Ferreiro & Pastoriza (2004).

Figure 1. Slit positions for AM 1219–430, AM 2030–303 and AM 2322–821 systems superimposed on the GMOS-S *r'* acquisition images.

Table 2. Nuclear separation (NS) between the individual galaxies of the galaxy pairs, galactocentric distance with surface brightness of 25 mag arcsec^{-2} (R_{25}), inclination angle (i) and the radial velocity (cz) of the objects in our sample.

ID		NS (kpc)	R_{25} (kpc)	i (°)	cz (km s^{-1})
AM 1054–325	A	–	6.98[a]	62[b]	3 788
	B	17	6.81[a]	54[b]	3 850
AM 1219–430	A	–	15.3[c]	50[c]	6 957
	B	33.7	6.2[c]	–	6 879
AM 1256–433	A	–	–	36[b]	9 215
		–	–	33[b]	9 183
	B	91.6	24.32[d]	77[d]	9 014
AM 2030–303	A	–	17.4[d]	23[d]	12 323
		–	–	–	12 465
	B	40.5	13.5[d]	35[d]	12 474
AM 2058–381	A	–	34.3[d]	68[d]	12 383
	B	44	16.7[d]	57[d]	12 460
AM 2229–735	A	–	26.1[d]	60[d]	17 535
	B	24.5	22.5[d]	48[d]	17 342
AM 2306–721	A	–	24.3[d]	56[e]	8 919
	B	52.6	15.6[d]	60[e]	8 669
AM 2322–821	A	–	13.5[d]	20[f]	3 680
	B	33.7	4.2[d]	63[f]	3 376

[a] Paturel et al. (1991).
[b] Paturel et al. (2003).
[c] Hernandez-Jimenez et al. (2013).
[d] Ferreiro, Pastoriza & Rickes (2008).
[e] Krabbe et al. (2008).
[f] Krabbe et al. (2011).

Gemini acquisition images in the *r* filter, using a simple isophotal fitting with the IRAF[1] `stsdas.ellipse` task. The same procedure was used by Krabbe et al. (2011).

We can see in Tables 1 and 2 that some galaxies in our sample have large inclinations, which could affect the derived abundance gradients. In fact, as pointed out by Sánchez et al. (2012), face-on galaxies are more suitable for studying the spatial distribution of the properties of H II regions. For example, if we assume an inclination angle *i* for a given galaxy larger than the real one, the abundance gradient derived would be steeper than the one obtained with the right *i* value. However, this effect is critical for isolated spiral galaxies, which have clear (or steep) abundance gradients, but it is not so important for objects with shallow gradients, such as interacting galaxies.

To obtain the nebular spectra not contaminated by the stellar population contribution, we use the stellar population synthesis code STARLIGHT (Cid Fernandes et al. 2005), following the methodology presented by Krabbe et al. (2011). A detailed analysis of the stellar population for the sample of objects will be presented in a future work (Rosa et al., in preparation). Once the stellar population contribution has been determined, the underlying absorption-line spectrum is subtracted from the observed spectra. Fig. 2 shows the spectrum of the region with the highest brightness of AM 1256–433 along PA = 325°, the synthesized spectrum and the pure emission

Paper I because of the low signal-to-noise ratio (S/N) of the [S II] $\lambda\lambda 6716, 6731$ emission lines needed to perform the electron density estimations. The observed spectra comprise the flux contained in an aperture of 1 arcsec × 1.152 arcsec. Considering a spatially flat cosmology with $H_0 = 71$ km s^{-1} Mpc^{-1}, $\Omega_{\mathrm{m}} = 0.270$, $\Omega_{\mathrm{vac}} = 0.730$ (Wright 2006) and the distances to the systems included in our sample, this corresponds to apertures between about 200 and 1100 pc on the plane of the galaxies. Therefore, the physical properties derived from these spectra represent the ones of a complex of H II regions. In Table 2, we present the nuclear separation between the components of the galaxy pairs, the galactocentric distances given in units of R/R_{25}, where R_{25} is the *B*-band isophote at a surface brightness of 25 mag arcsec^{-2}, the inclination angle (i) of each galaxy analysed and the references from which the information was taken. The inclination of each galaxy with respect to the plane of the sky was computed as $\cos(i) = b/a$, where a and b are the major and minor semi-axes of the galaxy, respectively. The a and b values, as well as the PA of the major axis of each galaxy, were obtained from the

---

[1] IRAF is distributed by the National Optical Astronomy Observatory, which is operated by the Association of Universities for Research in Astronomy (AURA), Inc., under cooperative agreement with the National Science Foundation.
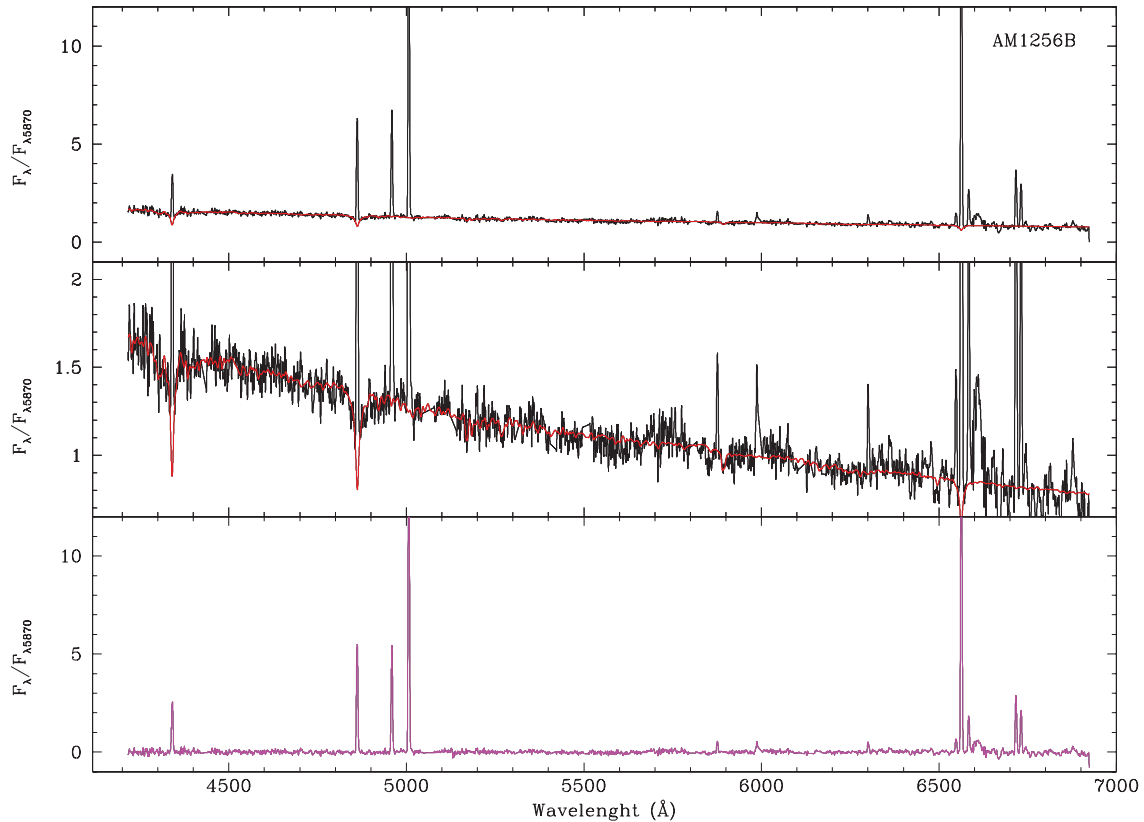
Figure 2. Stellar population synthesis for the brightest region of AM 1256B along PA = 325°. Top panel: reddening-corrected spectrum (black line) and the synthesized spectrum (red line). Middle panel: *y*-axis zoom of the top panel. Bottom panel: pure emission spectrum obtained as the difference between both spectra in the top panel.

spectrum corrected for reddening. The intensities of the emission lines Hβ, [O III] λ5007, Hα, [N II] λ6584 and [S II] $\lambda\lambda$6716, 6731 were obtained from the pure nebular spectrum of each aperture using Gaussian line profile fitting.

We used the IRAF `splot` routine to fit the lines, with the associated error given as $\sigma^2 = \sigma_{cont}^2 + \sigma_{line}^2$, where σ_{cont} and σ_{line} are the continuum rms and the Poisson error of the line flux, respectively. The residual extinction associated with the gaseous component for each spatial bin was calculated by comparing the observed value of the Hα/Hβ ratio to the theoretical value of 2.86 obtained by Hummer & Storey (1987) for an electron temperature of 10 000 K and an electron density of 100 cm^{-3}. This value for the electron density is in the range of the mean electron density values ($24 \lesssim N_e \lesssim 532$ cm^{-3}) found for interacting galaxies in Paper I. The correction for foreground dust was done by using the reddening law given by Cardelli, Clayton & Mathis (1989), assuming the specific attenuation $R_V = 3.1$. We considered only emission-line measurements whose S/N was higher than 8. The galactocentric distance in relation to R_{25}, the flux of Hβ, the extinction coefficient C(Hβ) and the emission-line intensities normalized to the flux of Hβ for the regions considered in the systems are presented in Table 3.

3 DETERMINATION OF THE OXYGEN ABUNDANCE GRADIENTS

Because emission lines sensitive to the electron temperature are not detected in the spectra of the objects in our sample, the metallicity of the gas phase, traced by the relative abundance of oxygen to

hydrogen (O/H), was estimated using calibrations based on strong emission lines.

Considering the emission lines observed in our sample, it is only possible to use the intensities of the emission lines defined as $N2 = \log([\text{N II}] \ \lambda 6584/\text{H}\alpha)$ and $O3N2 = \log[([\text{O III}] \ \lambda 5007/\text{H}\beta)/([\text{N II}] \ \lambda 6584/\text{H}\alpha)]$, proposed by Storchi-Bergmann, Calzetti & Kinney (1994) and Alloin et al. (1979), respectively, as O/H indicators. We used the relations between these indices and O/H, calculated using direct estimations of the oxygen electron temperatures (T_e method), proposed by Pérez-Montero & Contini (2009) and given by

$$12 + \log(\text{O/H}) = 0.79 \times N2 + 9.07 \tag{1}$$

and

$$12 + \log(\text{O/H}) = 8.74 - 0.31 \times O3N2. \tag{2}$$

These calibrations are very similar to the ones proposed by Pettini & Pagel (2004). The most recent update of this calibration was carried out by Marino et al. (2013), who used direct oxygen abundance measurements obtained from the CALIFA survey and other sources from the literature. Using multiwavelength analysis of a sample of starburst galaxies and data compiled from the literature, López-Sánchez & Esteban (2010) have shown that the *N*2 and *O*3*N*2 parameters provide acceptable results for objects with $12 + \log(\text{O/H}) > 8.0$. López-Sánchez & Esteban (2010) also found that empirical calibrations considering these indices give results that are about 0.15 dex higher than the oxygen abundances derived via the T_e method. Although this difference is similar to the uncertainties of oxygen abundances derived from the T_e method (e.g. Kennicutt et al. 2003; Hägele et al. 2008), it seems to vary with the regime

Table 3. Specific parameters and intensity of emission lines corrected by reddening (relative to Hβ = 100). Only the AM 1054B galaxy is shown here. The total list of galaxies is available as Supporting Information on the publisher's web site.

R/R_{25}	$\log[F(\mathrm{H}\beta)]^a$	$C(\mathrm{H}\beta)$	[O III] $\lambda5007$	Hα	[N II] $\lambda6584$	[S II] $\lambda6716$	[S II] $\lambda6731$
				AM 1054B			
0.00	−14.51	0.40	152 ± 27	278 ± 9	112 ± 6	24 ± 10	27 ± 7
0.04SW	−14.97	0.26	154 ± 22	281 ± 7	115 ± 5	28 ± 4	29 ± 4
0.04NE	−14.93	0.23	141 ± 21	282 ± 9	114 ± 6	37 ± 3	37 ± 7
0.08NE	−15.82	0.08	139 ± 11	285 ± 11	119 ± 8	–	–
0.13NE	−17.11	0.08	113 ± 19	285 ± 15	119 ± 11	–	–

^{a}Logarithm of the Hβ observed flux in erg s^{-1} cm^{-2}.
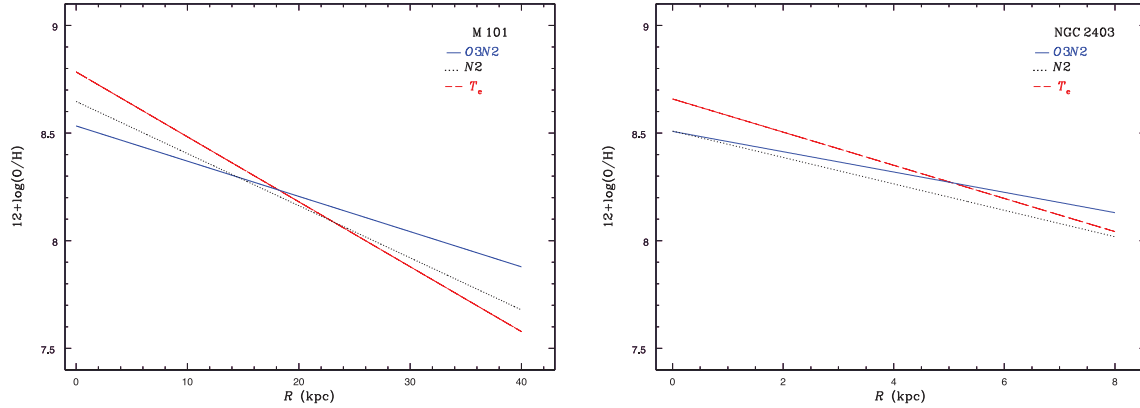
Figure 3. Oxygen abundance gradients computed via the $N2$ and $O3N2$ indices and direct estimations of the oxygen electron temperatures for the galaxies M101 (left) and NGC 2403 (right) using data taken from Kennicutt, Bresolin & Garnett (2003) and Garnett et al. (1997), respectively.

of metallicity (Dors et al. 2011). This can yield steeper oxygen gradients than the ones from the T_e method or an erroneous bend in the slope of abundance gradients (Pilyugin 2003). With the goal to compare O/H gradients derived using the $N2$ and $O3N2$ indices with the ones obtained from the T_e method, we have used data of H II regions located along the discs of the spiral galaxies M101 and NGC 2403, obtained by Kennicutt et al. (2003) and Garnett et al. (1997), respectively. Fig. 3 shows these gradients, and we can see that the gradients derived from the indices are shallower than the ones from the T_e method.

Scarano, Lépine & Marcon-Uchida (2011) and Bresolin et al. (2012) have pointed out that gradients are less affected by uncertainties in oxygen estimations yielded by the calibration of strong emission lines. However, it can be seen in Fig. 3 that the value of the O/H extrapolated for the central region of the galaxies ($R = 0$), obtained using different methods, can differ by up to 0.4 dex. This difference is higher than the uncertainty attributed to the O/H estimations using strong emission-line calibrations (Kewley & Ellison 2008). Similar results were found by Bresolin (2011) when comparing the oxygen gradient for NGC 4258 using theoretical calibrations by McGaugh (1991) and empirical calibrations by Pilyugin & Thuan (2005). The latter provides results essentially in agreement with those obtained from the T_e method (see also Pilyugin, Grebel & Mattsson 2012).

4 RESULTS

Figs 4–11 present the oxygen abundance determinations along the discs of the galaxies of our sample, obtained using equations (1) and (2), and linear regression fits to these data. Table 4 presents the

slopes of these fits and the values of 12+log(O/H) central ($R = 0$) for the galaxies for which only a global gradient represents well the O/H disc distribution (i.e. no bi-modal gradient behaviour was derived). It can be noted that in most cases, shallow gradients are derived in the interacting galaxies. The average values of the global gradients calculated for the close pairs in our sample are −0.10 ± 0.19 [dex/(R/R_{25})] and −0.15 ± 0.31 [dex/(R/R_{25})] using the $N2$ and $O3N2$ indices, respectively. These values are in agreement with the mean gradient −0.25 ± 0.02 [dex/(R/R_{25})] derived by Kewley et al. (2010) and they are shallower than the mean metallicity gradient −0.57 ± 0.19 [dex/(R/R_{25})] derived for 11 isolated spiral galaxies by Rupke, Kewley & Chien (2010b). Using the CALIFA data survey, Sánchez et al. (2014) have presented a study of galaxies with different interaction stages in order to study the effect on the abundance gradient. This study has a stronger statistical significance than previous studies. Sánchez et al. (2014) have shown the distribution of slopes of the abundance gradients derived for the different classes based on the interaction stages. From this analysis, they have found that galaxies with no evidence of interaction have an average value for the gradient of −0.11 dex/r_e and objects with evidence for early or advanced interactions have a slope of −0.05 dex/r_e, where r_e is the effective radius of the disc. This result confirms our findings and those obtained by Kewley et al. (2010). In what follows, the results obtained for each system are discussed separately.

4.1 AM 1054–325

This system is composed of two galaxies, one main galaxy AM 1054A and another secondary AM 1054B. Using the diagnostic diagram [O III] $\lambda5007$/Hβ versus [O I] $\lambda6300$/Hα, we have found (see
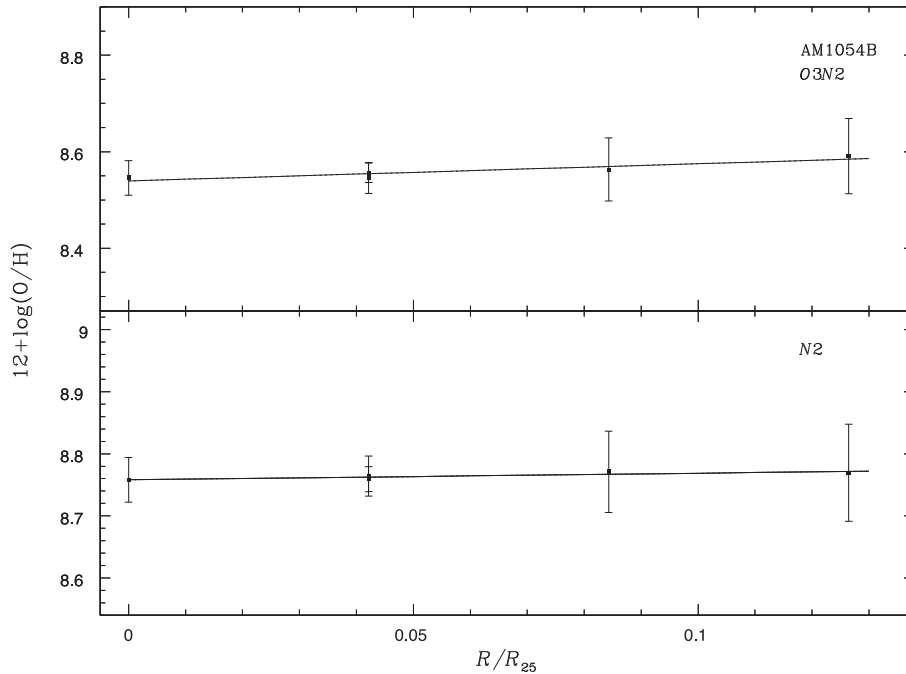
Figure 4. Oxygen abundance estimations along the disc of AM 1054B versus the galactocentric distance given in R/R_{25}. Points represent oxygen estimations obtained via the $N2$ (lower panel) and $O3N2$ (upper panel) indices. Lines represent a linear regression fit to our estimations whose coefficients are given in Table 4.

Paper I) that almost all H II regions located in the disc of AM 1054A have emission lines excited by shock gas. Therefore, abundance determinations were not performed for this object because shocks alter the ionization in such a way that the abundance calibrators cannot be used because they are calibrated for H II regions dominated by photoionization by young stars.

Fig. 4 shows the O/H distribution versus the galactocentric radius R normalized by R_{25} for AM 1054B. We have found gradient slopes of 0.11 ± 0.04 and 0.36 ± 0.04 dex/(R/R_{25}), with the central $12+\log(O/H)$ value being 8.54 (± 0.01) and 8.75 (± 0.06) dex from the $N2$ and $O3N2$ indices, respectively. AM 1054B is the only object in our sample for which both estimations of the central oxygen abundances are not in agreement with themselves within the errors (see Table 4). However, as can be seen in Fig. 4, the slopes were obtained using few points. Hence, the gradient determination is highly uncertain, although the current data indicate a flat O/H distribution.

4.2 AM 1219–430

This system is composed of the main galaxy AM 1219A and a secondary galaxy AM 1219B. Because it was not possible to measure the [O III] $\lambda 5007$ emission line with enough S/N in our spectrum of AM 1219B, for this object, O/H was estimated only using $N2$. We corrected by inclination the galactocentric distances for the main galaxy AM 1219A, considering $i = 50°$.

Fig. 5 shows the O/H distribution in both galaxies. For AM 1219B, we derived a slope $+0.10 \pm 0.18$ and a central oxygen abundance of 8.89 ± 0.04 dex. Similar to AM 1054B, the slope for AM 1219B was derived with few points (and with a large dispersion), which means the result is highly uncertain. For AM 1219A, the estimated oxygen gradient slopes are -0.29 ± 0.04 and -0.54 ± 0.04 using the $N2$ and $O3N2$ indices, respectively, with a central value of $12+\log(O/H) \sim 8.8$ derived from both indices. For values of R/R_{25}

from about 0.4 to 0.5, we can see a larger dispersion in the oxygen distribution than found at other galactocentric distances. Regions at this distance range, as can be seen in Fig. 1, are located in the intersections of the slits and are regions with high surface brightness. It can be noted in Fig. 5, for AM 1219A, that there is a change in the slope at about $R/R_{25} = 0.5$. The slopes of the abundance gradient in the inner disc ($R/R_{25} < 0.5$) considering the $O3N2$ and $N2$ indices are -0.64 ± 0.05 and -0.21 ± 0.05, respectively. For the outer region ($R/R_{25} > 0.5$), the slopes are $+0.20 \pm 0.11$ and $+0.16 \pm 0.11$ using $O3N2$ and $N2$, respectively.

4.3 AM 1256–433

As reported in Paper I, the AM 1256–433 system is composed by three galaxies and we only observed the AM 1256–433B component. For this object, the galactocentric distance measurements were corrected by inclination considering $i = 77°$. Fig. 6 shows the O/H distribution via the $N2$ and $O3N2$ indices. We obtained gradient slopes of -0.85 ± 0.06 and -0.71 ± 0.06 for these indices, respectively, with a central $12+\log(O/H)$ value of ~ 8.7 dex. Interestingly, we can note a steeper oxygen gradient for $R/R_{25} < 0.27$ than the one obtained for the outer regions. The slopes of the abundance gradient in the inner disc considering the $N2$ and $O3N2$ indices are -0.78 ± 0.13 and -0.93 ± 0.07. For the outer disc ($R/R_{25} > 0.27$) we derived for the $N2$ and $O3N2$ indices the slopes -0.55 ± 0.10 and -0.30 ± 0.08, respectively. The slopes of the global fits to the abundance estimations are dominated by the values of the outer regions of the galaxy, and they are slightly steeper than the ones obtained only considering these outer regions.

4.4 AM 2030–303

This system is composed of three galaxies, a main galaxy AM 2030A (ESO 463-IG 003 NED01), ESO 463-IG 003 NED02 and
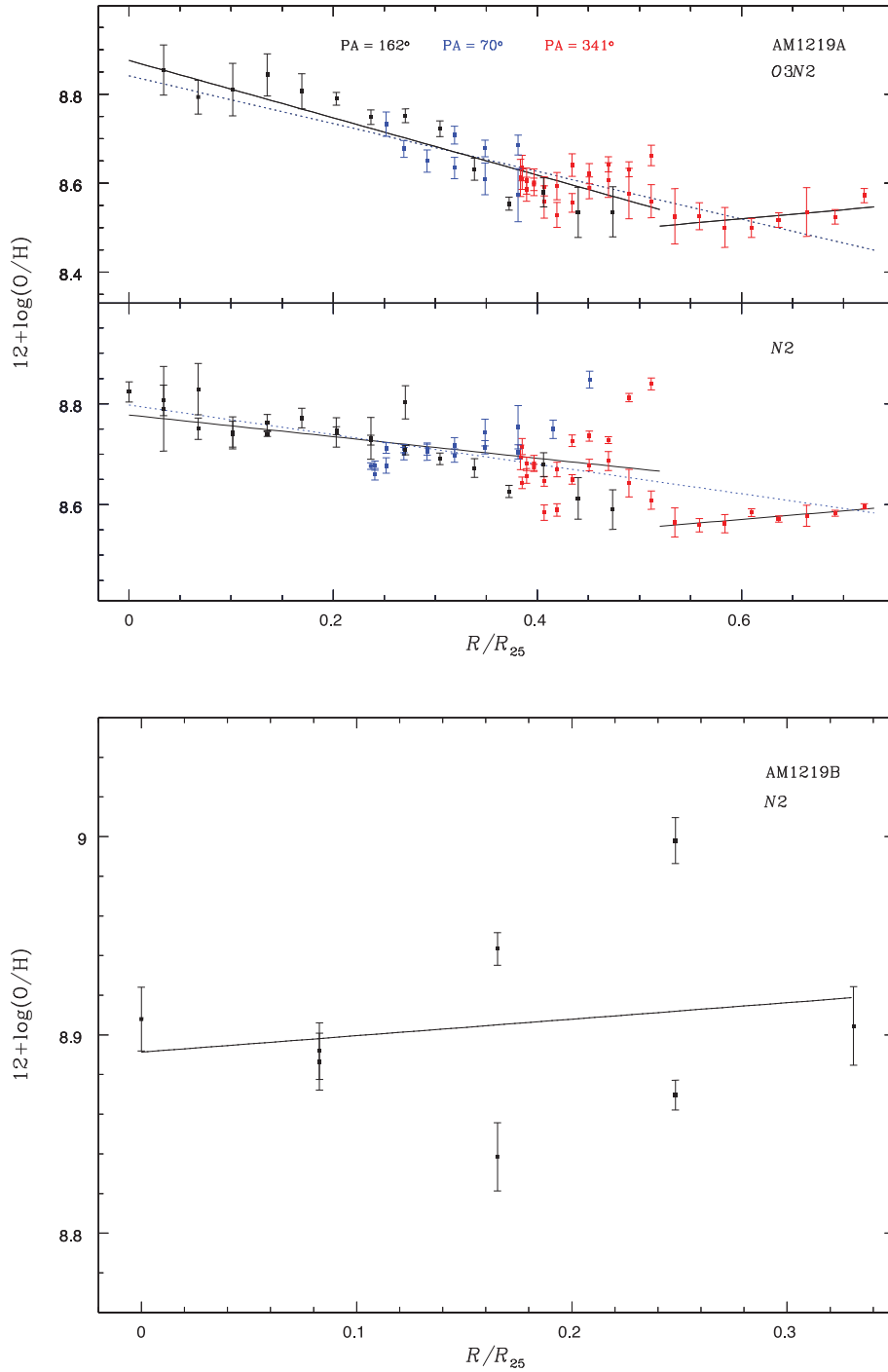
Figure 5. Same as Fig. 4 but for AM 1219A and AM 1219B. For AM 1219A, the determinations for the regions observed in different long-slit positions are indicated for distinct colours, as indicated. Also shown are linear regressions considering all regions along the disc (dotted blue line) and inner and outer regions to galactocentric distance $R/R_{25} = 0.5$ (solid black line).

ESO 463-IG 003 NED03. These last two objects are a subsystem called AM 2030B. Fig. 1 shows the slit positions for each object. We corrected by inclination the galactocentric distances of AM 2030B considering $i = 35°$. Because of the low number of H II regions observed, it was not possible to compute the O/H gradient for ESO 463-IG 003 NED002. Fig. 7 presents the results for AM 2030A and AM 2030B.

For AM 2030A, considering global fits, we obtained a central value $12+\log(O/H) = 8.73 \pm 0.10$ with a slope -0.31 ± 0.30 using $N2$ and 8.62 ± 0.07 and -0.22 ± 0.20 using $O3N2$. These values are similar to the highest O/H value obtained for the H II region CDT1 in NGC 1232 by Castellanos, Díaz & Terlevich (2002). Now, considering an abundance gradient break, the slopes for the inner disc ($R/R_{25} < 0.27$) obtained via the $N2$ and $O3N2$ indices are
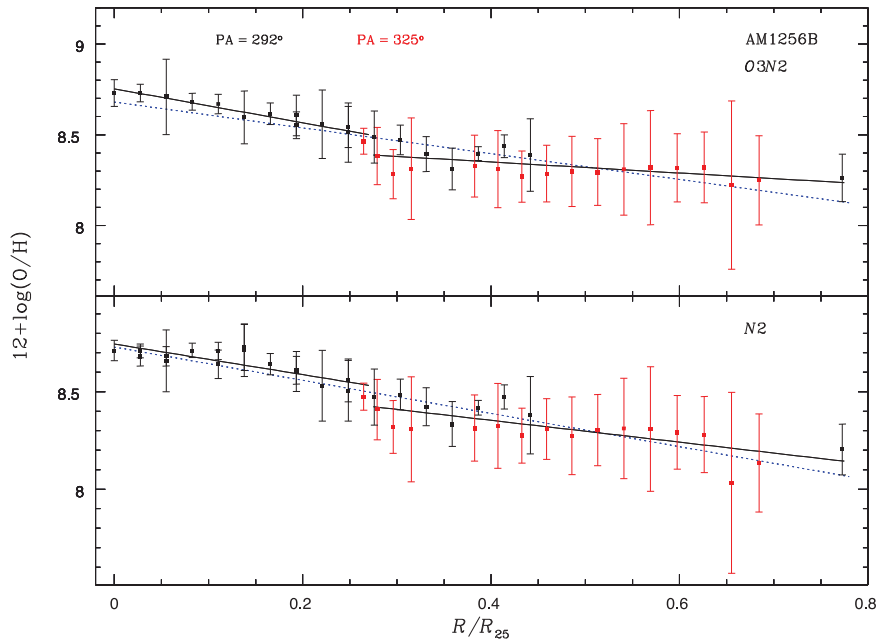
Figure 6. Same as Fig. 5 but for AM 256B. Linear regressions are shown considering all regions along the disc (dotted blue line) and inner and outer regions to galactocentric distance $R/R_{25} = 0.35$ (solid black line).

-0.27 ± 0.46 and -0.95 ± 0.27, respectively. For the outer disc ($R/R_{25} > 0.27$), we derived for the $N2$ and $O3N2$ indices the slopes -0.47 ± 0.01 and 0.00 ± 0.45, respectively.

For AM 2030B (ESO 463-IG 003 NED003), we found two different O/H abundance distributions at the inner and outer regions of $R/R_{25} = 0.2$. The slopes of the abundance gradient in the inner disc ($R/R_{25} < 0.17$) considering the $N2$ and $O3N2$ indices are $+1.85 \pm 0.43$ and $+0.92 \pm 0.22$, respectively. For the outer disc ($R/R_{25} > 0.17$), we derived for the $N2$ and $O3N2$ indices the slopes -0.28 ± 0.25 and -0.17 ± 0.18, respectively.

4.5 AM 2058–381

For this system, the O/H gradient was only determined for one galaxy, AM 2058A, because the H II regions of its companion galaxy, AM 2058B, have emission lines excited by gas shock (see Paper I). Fig. 8 shows the oxygen distribution, where the galactocentric distances were corrected considering $i = 68°$. We found a slope for the O/H gradient from the $N2$ index of -0.29 ± 0.08 with $12+\log(O/H) = 8.79 \pm 0.02$ for the central region. Using the $O3N2$ index, we found -0.35 ± 0.08 and 8.78 ± 0.02 dex.

4.6 AM 2229–735

We obtained the O/H abundance distributions only for the main galaxy of the system AM 2229–735, namely AM 2229A, and these are shown in Fig. 9. The galactocentric distances for this object were corrected by inclination considering $i = 48°$. For estimations via the $N2$ index, we found a slope of of 0.03 ± 0.09 with central oxygen abundance $12+\log(O/H) = 8.71 \pm 0.03$ dex. For the $O3N2$ index, these values are -0.11 ± 0.06 and 8.70 ± 0.02 dex.

4.7 AM 2306–721

This pair is composed of a main galaxy AM 2306A and a companion galaxy AM 2306B. The O/H gradient (see Fig. 10) was determined

only for the main galaxy AM 2306A because, for its companion, AM 2306B, the presence of gas shock excitation along the disc was found (see Paper I). By using the $N2$ index, we found a slope of -0.40 ± 0.05 and a central value $12+\log(O/H) = 8.81 \pm 0.02$ dex. Using the $O3N2$ index, the values -0.57 ± 0.06 and 8.83 ± 0.02 dex were found.

4.8 AM 2322–821

Fig. 11 shows the O/H distributions along the disc of the pair of galaxies AM 2322A and AM 2322B. For AM 2322A, a correction for inclination was performed considering $i = 20°$. For AM 2322A, by using the $N2$ index, we obtained a slope of -0.17 ± 0.01 and a $12+\log(O/H) = 8.79 \pm 0.01$ dex for the central part. From the $O3N2$ index, these values were found to be -0.19 ± 0.01 and 8.77 ± 0.01 dex. For the secondary object AM 2322B, the use of the $N2$ index yielded -0.14 ± 0.05 and 8.57 ± 0.20 dex for the central part, while the use of the $O3N2$ index yielded -0.07 ± 0.05 and 8.53 ± 0.20 dex.

5 DISCUSSION

Determinations of the oxygen abundance gradients in interacting galaxies have shown that these are shallower than the ones in isolated galaxies. This result was obtained recently and few works have addressed this subject. In what follows, we summarize some studies that have taken this direction.

(i) Krabbe et al. (2008) obtained long-slit spectroscopy data with Gemini/GMOS of the two components (A and B) of the galaxy pair AM 2306–721. They used a comparison between the observed emission-line ratio intensities (R_{23} and [O II] $\lambda3727$/[O III] $\lambda5007$; see McGaugh 1991) and those predicted by photoionization models to determine the metallicity gradient. They found a clear gradient
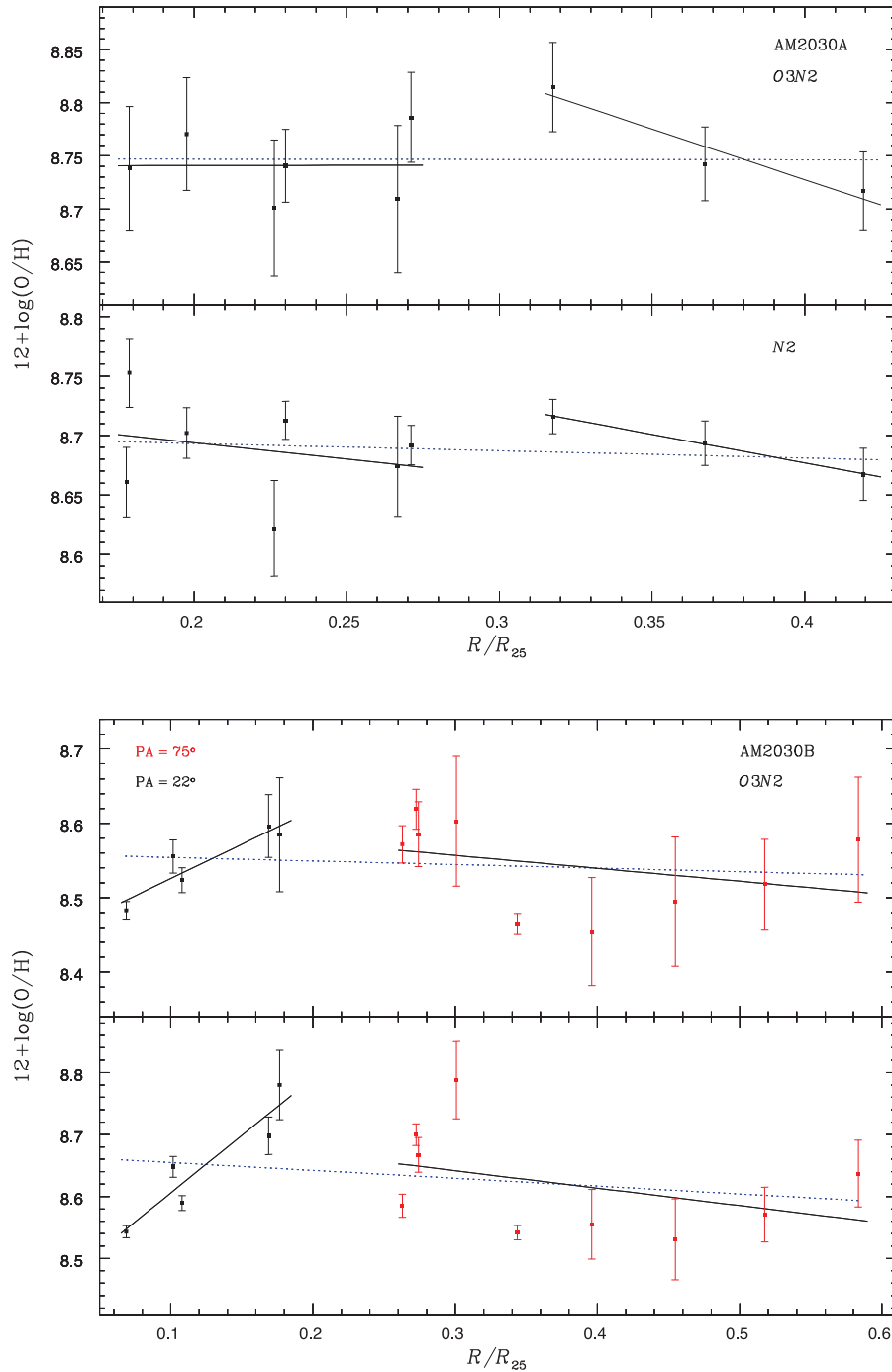
Figure 7. Same as Fig. 5 but for AM 2030A and AM 2030B (ESO 463-IG 003 NED003). Linear regressions are shown considering all regions along the disc (dotted blue line) and inner and outer regions to the galactocentric distance $R/R_{25} = 0.2$ (solid black line).

for the most massive object of the pair, AM 2306A, while for AM 2306B, they found an oxygen abundance relatively homogeneous across the disc.

(ii) Kewley et al. (2010) selected five sets of close pairs with separation between 15 and 25 kpc from the sample of Barton et al. (2000) and they obtained spectra for 12–40 star-forming regions in eight of the close pair galaxies using the Keck Low-Resolution Imaging Spectrograph. This work was the first systematic investigation of metallicity gradients in close pairs. Kewley et al. (2010) found that

the metallicity gradients in their sample are significantly shallower than the gradients in isolated spiral galaxies. They used a theoretical calibration between the [N II] λ6584/[O II] λ3727 emission-line ratio and the metallicity.

(iii) Krabbe et al. (2011) obtained spectroscopic data of the two components (A and B) of the system AM 2322–821 with Gemini/GMOS. The oxygen gradient was derived following the same procedure as that in Krabbe et al. (2008), and a flat oxygen gradient was derived for both galaxies.
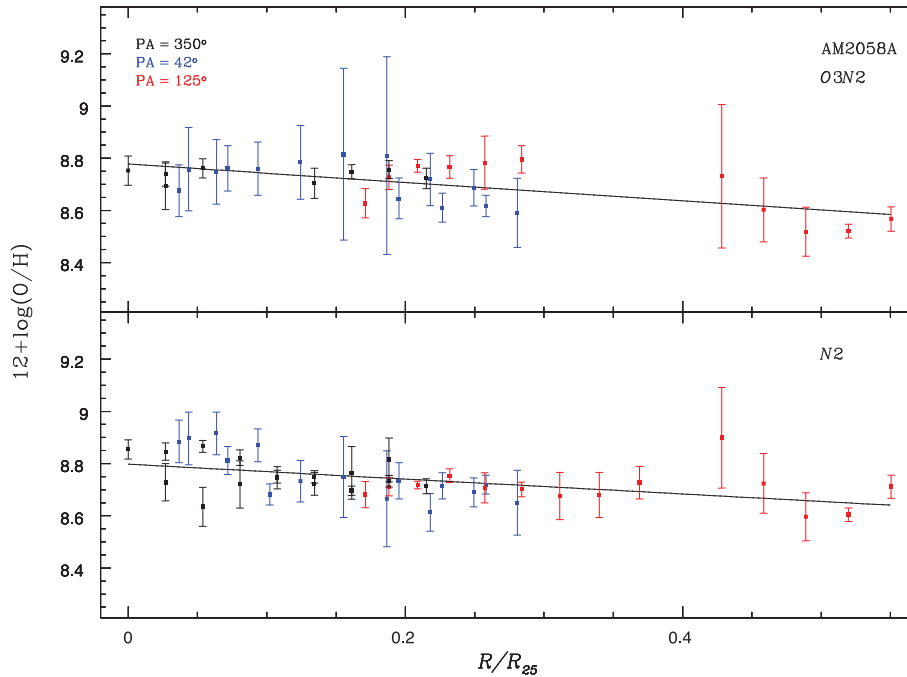
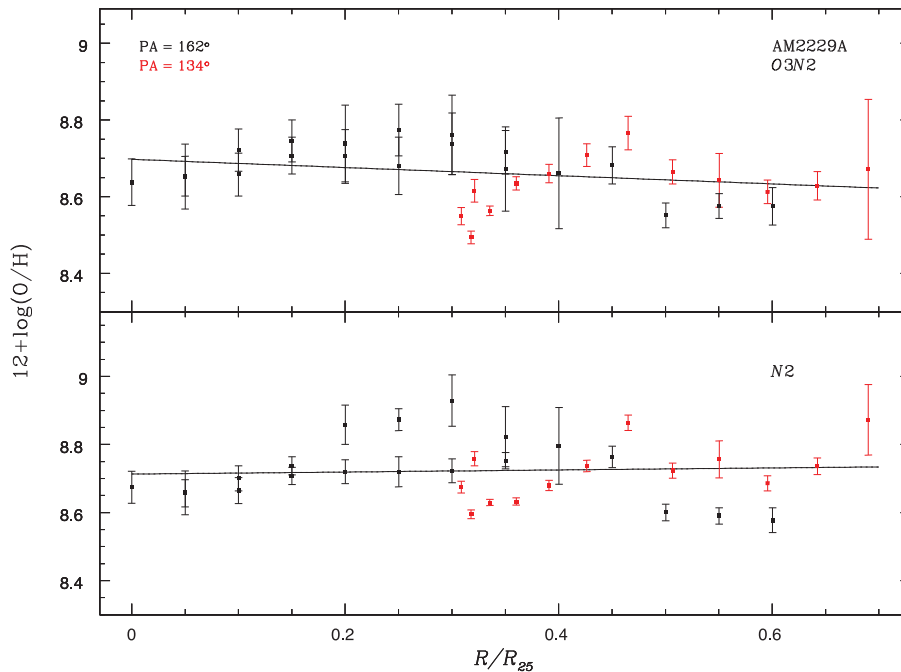**Figure 8.** Same as Fig. 5 but for AM 2058A.

Figure 9. Same as Fig. 5 but for AM 2229A.

(iv) Using the Focal Optical Reducer and Spectrograph (FORS2) attached to the Very Large Telescope, Bresolin et al. (2012) obtained optical spectroscopy of H II regions belonging to NGC 1512. This galaxy has a companion, NGC 1510, separated by about 13.8 kpc. A flat radial abundance gradient was also obtained by using several calibrations based on strong lines, as well as some oxygen abundance determinations using the T_e method.

(v) Torres-Flores et al. (2014) obtained Gemini/GMOS spectroscopic data of the interacting galaxy NGC 92, which is part of a compact group and displays an extended tidal tail. They used calibrations of the $N2$, $O3N2$ and [Ar III] $\lambda7136$/[O III] $\lambda5007$ indices proposed by Pettini & Pagel (2004) and Stasińska (2006) to estimate the O/H abundance. Torres-Flores et al. (2014) found that most of the regions in NGC 92 present a similar oxygen abundance, which
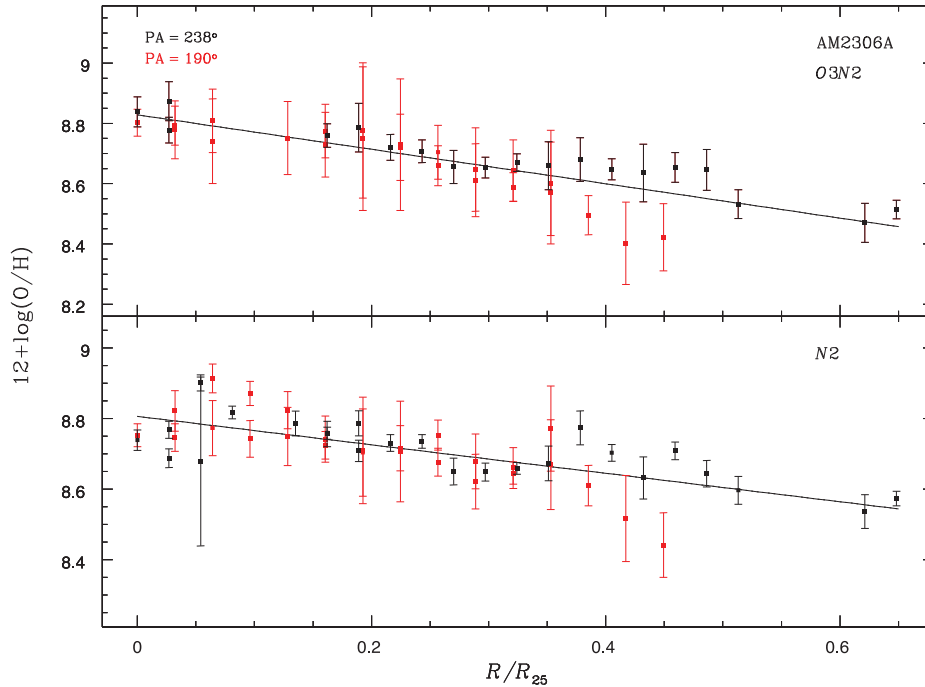
Figure 10. Same as Fig. 5 but for AM 2306A.

produces an almost flat metallicity gradient, with a possible break in this gradient for the galactocentric distance of ∼10 kpc.

(vi) Most recently, based on the largest and better defined statistical sample of galaxies yielded by the CALIFA survey, Sánchez et al. (2014) have compared the O/H abundance gradients of about 300 nearby galaxies, with more than 40 mergers/interacting systems, half of which are galaxy pairs. They found, for the first time, clear statistical evidence of a flattening in the abundance gradients in the interacting systems at any interaction stage, in agreement with the previous results.

From the literature summarized above, it can be seen that oxygen gradients have been determined for close pairs or merger systems mainly using different strong emission-line calibrations and some few determinations using the T_e method. In this paper, we have performed a new determination of the O/H gradients for the galaxies AM 2306A and AM 2322A–B previously studied by Krabbe et al. (2008, 2011) and we have presented an analysis of eight more galaxies in close pairs. Fig. 12 shows the oxygen gradients from *N*2 derived for our sample, for the galaxies in the pairs from the literature cited above, and for the four isolated galaxies, also from the literature. We can see that the oxygen gradients derived for the objects in our sample are shallower than those in isolated spirals. Although most of the slopes of these gradients are in agreement with the ones obtained by Kewley et al. (2010), we found lower O/H abundances for the central parts of the galaxies. This is a result of the oxygen abundance estimations via theoretical calibrations, such as the one used by Kewley et al. (2010), which yield higher values than the ones from calibrations based on oxygen estimations via the T_e method (e.g. Dors & Copetti 2005). Krabbe et al. (2008), Kewley et al. (2010) and, most recently, Sánchez et al. (2014) interpreted the absence of an abundance gradient in interacting galaxies as a result of the mixing produced by low-metallicity gas from the outer parts combining with the metal-rich gas of the centre of the galaxy. Here we have confirmed this result by increasing the sample of objects.

As we pointed out in Section 4, a flattening in the oxygen gradient was found in the outer part of AM 1256B from $R/R_{25} \approx 0.35$ ($R \approx$ 8.5 kpc), in AM 1219A from $R/R_{25} \approx 0.5$ ($R \approx 7.6$ kpc) and AM 2030B from $R/R_{25} \approx 0.2$ ($R \approx 2.7$ kpc). In the case of AM 1219A and AM 1256B, the inner gradients have negative slopes while AM 2030B presents a positive inner gradient. In contrast, AM 2030A has a positive-slope outer gradient while the inner gradient is almost compatible with a flat behaviour, with the break at about $R/R_{25} \approx$ 0.3 ($R \approx 5$ kpc). However, if we take into account the errors in the measurements, in the latter case the slope of the outer gradient is also compatible with zero, although because of the low number of H II regions in the outer zone, we are not able to give a conclusion. The flattening in the oxygen gradients in the outer part was also found for individual galaxies (Martin & Roy 1995; Bresolin et al. 2009b; Goddard et al. 2011; Rosales et al. 2011; Zahid & Bresolin 2011; Bresolin et al. 2012; Marino et al. 2012; Torres-Flores et al. 2014; Rodríguez-Baras et al. 2014; Miralles-Caballero et al. 2014), a small sample of interacting galaxies (Werk et al. 2011), a large sample of objects (Sánchez et al. 2012, 2014), and even for the Milky Way (Esteban et al. 2013). Basically, there are four theoretical scenarios to explain the flattening of the oxygen abundance gradients at a given galactocentric distance:

(i) the pumping out effect of corotation, which produces gas flows in opposite directions on the two sides of the resonance, yielding a minimum metallicity (Scarano & Lépine 2013) and SFR (Mishurov, Lépine & Acharova 2002);

(ii) a decrease of the star-formation efficiency as proposed by Esteban et al. (2013);

(iii) the accretion of pristine gas (Marino et al. 2012; Sánchez et al. 2014);

(iv) the bar presence (e.g. Zaritsky et al. 1994; Martin & Roy 1994).

The data in our sample only allow us to investigate the bar presence and the SFR rate along the galactic discs. An inspection in
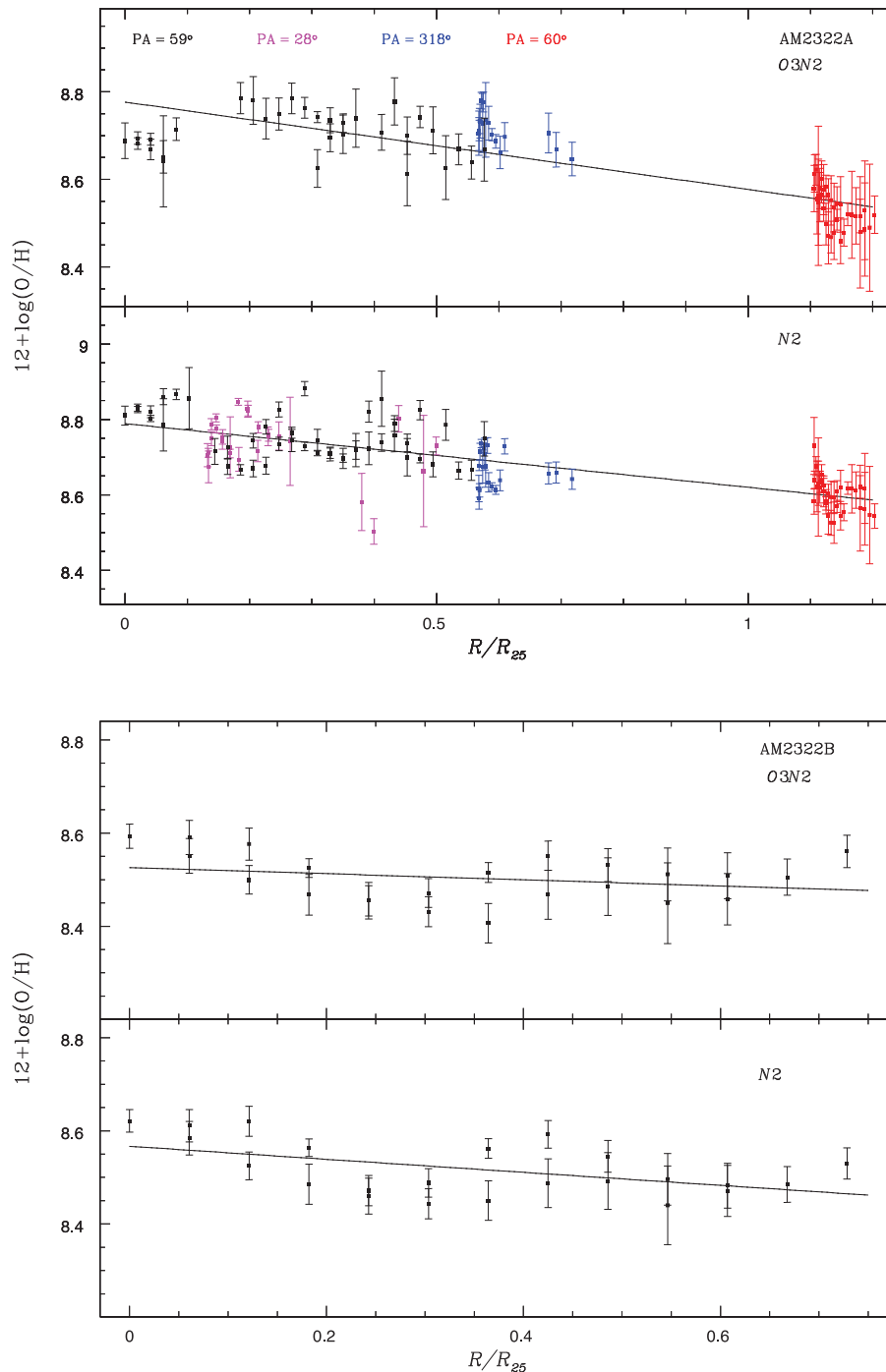
Figure 11. Same as Fig. 5 but for AM 2322A and AM 2322B.

the GMOS-S r' acquisition images of AM 1256B, AM 1219A, AM 2030A and AM 2030B does not reveal the presence of any bar. Moreover, Sánchez et al. (2014) investigated the effects of bars in the abundance gradients for the objects observed in the CALIFA survey, and did not find differences between the statistical term for the slope of the abundance gradient for barred galaxies and the one for other objects. Therefore, we have excluded the bar presence as an explanation for the flattening found in these four interacting galaxies of our sample.

To investigate whether there is a minimum SFR at the break region, we have used the Hα flux measured in our observation and the relation given by Kennicutt (1998):

$$\mathrm{SFR}(\mathrm{M}_\odot\,\mathrm{yr}^{-1}) = 7.9 \times 10^{-42}\, L(\mathrm{H}\alpha)(\mathrm{erg\,s^{-1}}). \qquad (3)$$

Because the absolute flux of Hα was not obtained, our SFR values must be interpreted as a relative estimation and the present analysis is only useful to study the behaviour of the SFR along the AM 1256B, AM 1219A, AM 2030A and AM 2030B discs.

Table 4. Slope of the oxygen abundance gradient and the central value derived for the objects in our sample with no bi-modal gradient behaviour.

Object	N2		O3N2	
	Slope [dex/(R/R_{25})]	12+log(O/H)$_{Central}$	Slope [dex/(R/R_{25})]	12+log(O/H)$_{Central}$
AM 1054B	+0.11 ± 0.04	8.54 ± 0.01	+0.36 ± 0.04	8.75 ± 0.06
AM 1219B	+0.10 ± 0.18	8.89 ± 0.04	–	–
AM 2058A	−0.29 ± 0.08	8.79 ± 0.02	−0.35 ± 0.08	8.78 ± 0.02
AM 2229A	+0.03 ± 0.09	8.71 ± 0.03	−0.11 ± 0.06	8.70 ± 0.02
AM 2306A	−0.40 ±0.05	8.81 ± 0.02	−0.57 ± 0.06	8.83 ± 0.02
AM 2322A	−0.17 ± 0.01	8.79 ± 0.01	−0.18 ± 0.02	8.77 ± 0.01
AM 2322B	−0.14 ± 0.05	8.57 ± 0.02	−0.07 ± 0.05	8.53 ± 0.02
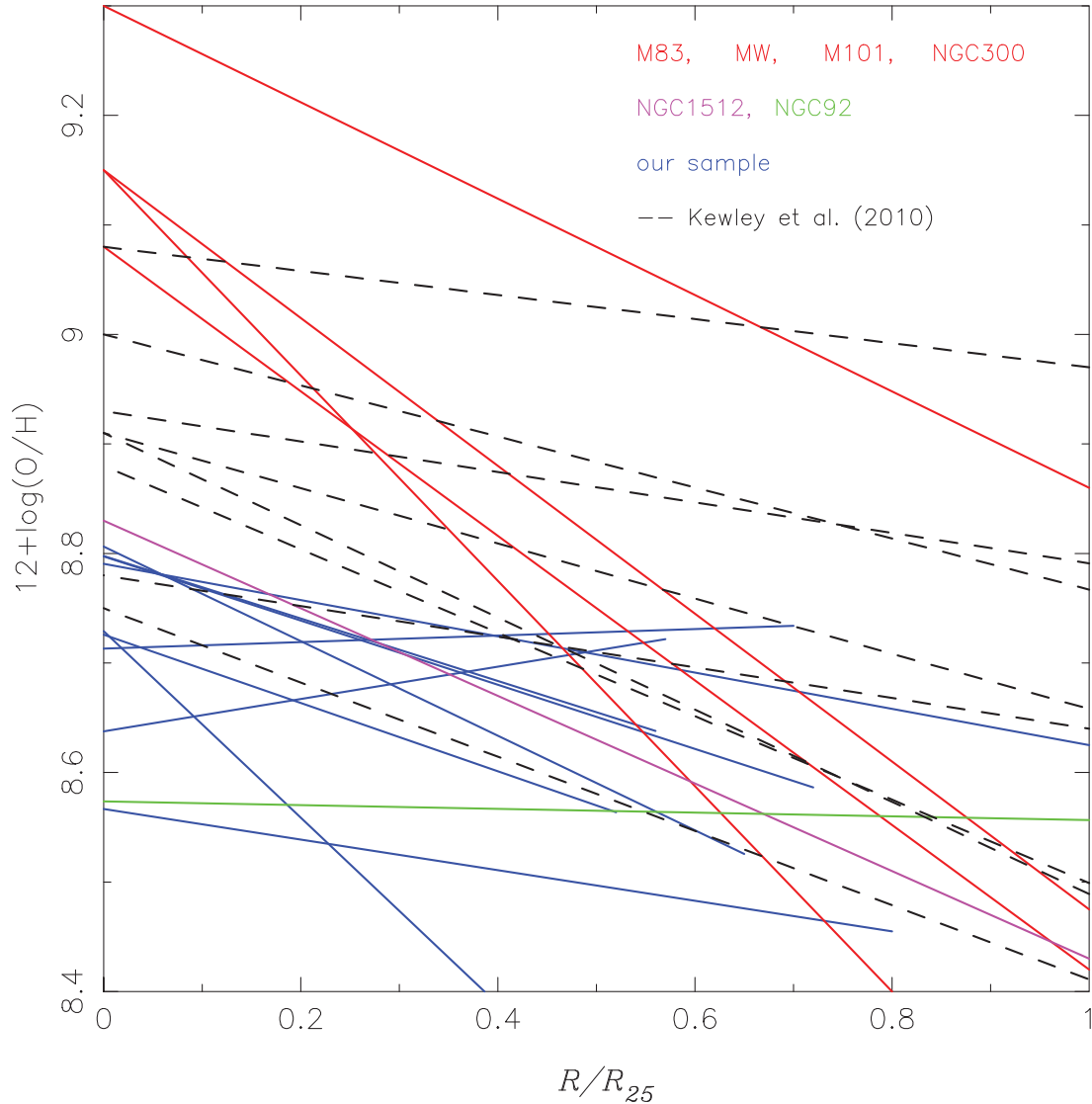
Figure 12. Metallicity gradients from *N2* for our sample. The gradients for AM 1219B and AM 1054B, derived with few points (see text), are not shown. For comparison, we show the metallicity gradients for the isolated galaxies M101, Milky Way, M83 and NGC 300 (whose data are taken from Kennicutt et al. 2003, Shaver et al. 1983, Bresolin et al. 2005 and Bresolin et al. 2009b, respectively), eight interacting galaxies presented by Kewley et al. (2010), NGC 92 (Torres-Flores et al. 2014) and NGC 1512 (Bresolin et al. 2012).

Fig. 13 shows the SFR versus R/R_{25} for the galaxies above, and the inner region where the steeper gradient was found is indicated. For two objects, AM 1219A and AM 2030B, we can see that the SFR minimum values are located very close to the regions where the oxygen gradient breaks, in agreement with Esteban et al. (2013). For AM 1219A only, we also found a minimum in the estimated metallicities, indicating that this break zone could be associated with a corotation radius, as pointed out by Mishurov et al. (2002).
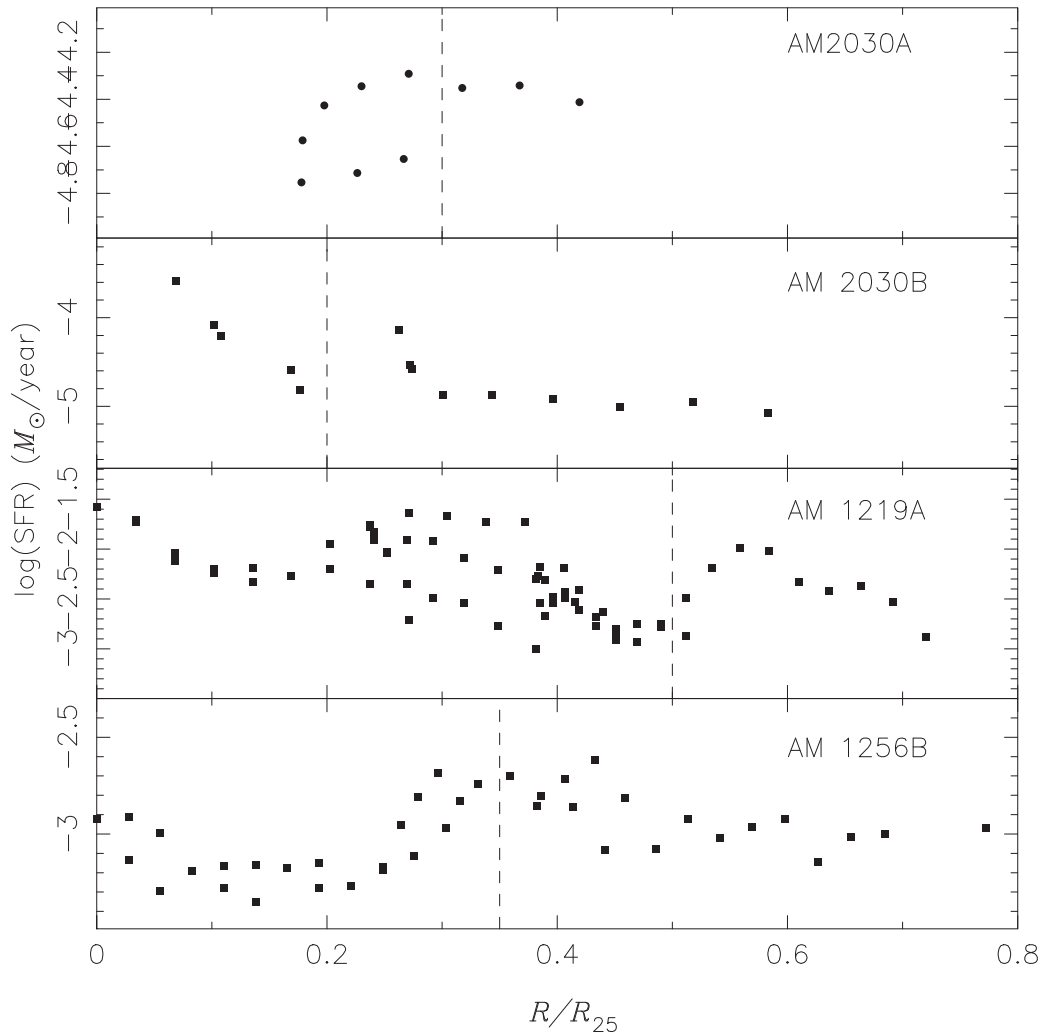
Figure 13. SFR versus the galactocentric distance (R/R_{25}) for AM 1256B, AM 1219A, AM 2030B and AM 2030A. The dotted line separates the inner region where the steeper gradient was found (see text).

For the other two objects, AM 1256B and AM 2030A, the breaks in the abundance gradients are located very close to the SFR maximum.

Another important issue is the behaviour of the ionization parameter U with the metallicity. Basically, U represents the dimensionless ratio of the ionizing photon density to the electron density and it is defined as $U = Q_{\rm ion}/4\pi R_{\rm in}^2 nc$, where $Q_{\rm ion}$ is the number of hydrogen ionizing photons emitted per second by the ionizing source, $R_{\rm in}$ is the distance from the ionization source to the inner surface of the ionized gas cloud (in cm), n is the particle density (in cm^{-3}) and c is the speed of light. Therefore, because the gas flow along the disc of interacting galaxies yields high values of electron density when compared to the ones found in isolated star-forming regions (Paper I), we expect to find low U values in the H II regions located in our sample. To verify this, we used the spectroscopic data presented in Table 3 and the relation,

$$\log U = -1.66(\pm 0.06) \times S2 - 4.13(\pm 0.07), \qquad (4)$$

taken from Dors et al. (2011), where $S2 = \log[$ [S II] ($\lambda\lambda 6717$, 6731)/Hα]. This equation is valid for $-1.5 \lesssim \log U \lesssim -3.5$ and estimations out of this range were not considered. These U estimations are plotted in Fig. 14 versus the O/H abundances determined from $N2$ for our sample, for H II regions in the interacting galaxy NGC 1512 observed by Bresolin et al. (2012). We also plot estimations for star-forming regions in isolated galaxies obtained using the same calibrations and the data compiled by Dors et al. (2011). The CALIFA data (Sánchez et al. 2012) for about 300 galaxies of any morphological type are also included in this analysis. It can be seen that H II regions located in interacting galaxies do not present the lowest U values. However, there is a clear correlation indicating that the highest abundances are found in those regions of galaxies with lower ionization strength (see also Freitas-Lemes et al. 2013; Pérez-Montero 2014). In fact, the H II regions located in the centre of galaxies are more evolved (from their Hα equivalent width) than those located in the outer regions, as pointed out by Sánchez et al. (2012); these have lower and higher ionization strengths, respectively.

6 CONCLUSIONS

We have presented an observational study of the oxygen gradient abundance in interacting galaxies. Long-slit spectra in the range 4400–7300 Å were obtained with the GMOS-S for 11 galaxies in eight close pairs. Spatial profiles of oxygen abundance (used as a metallicity tracer) in the gaseous phase along galaxy discs were
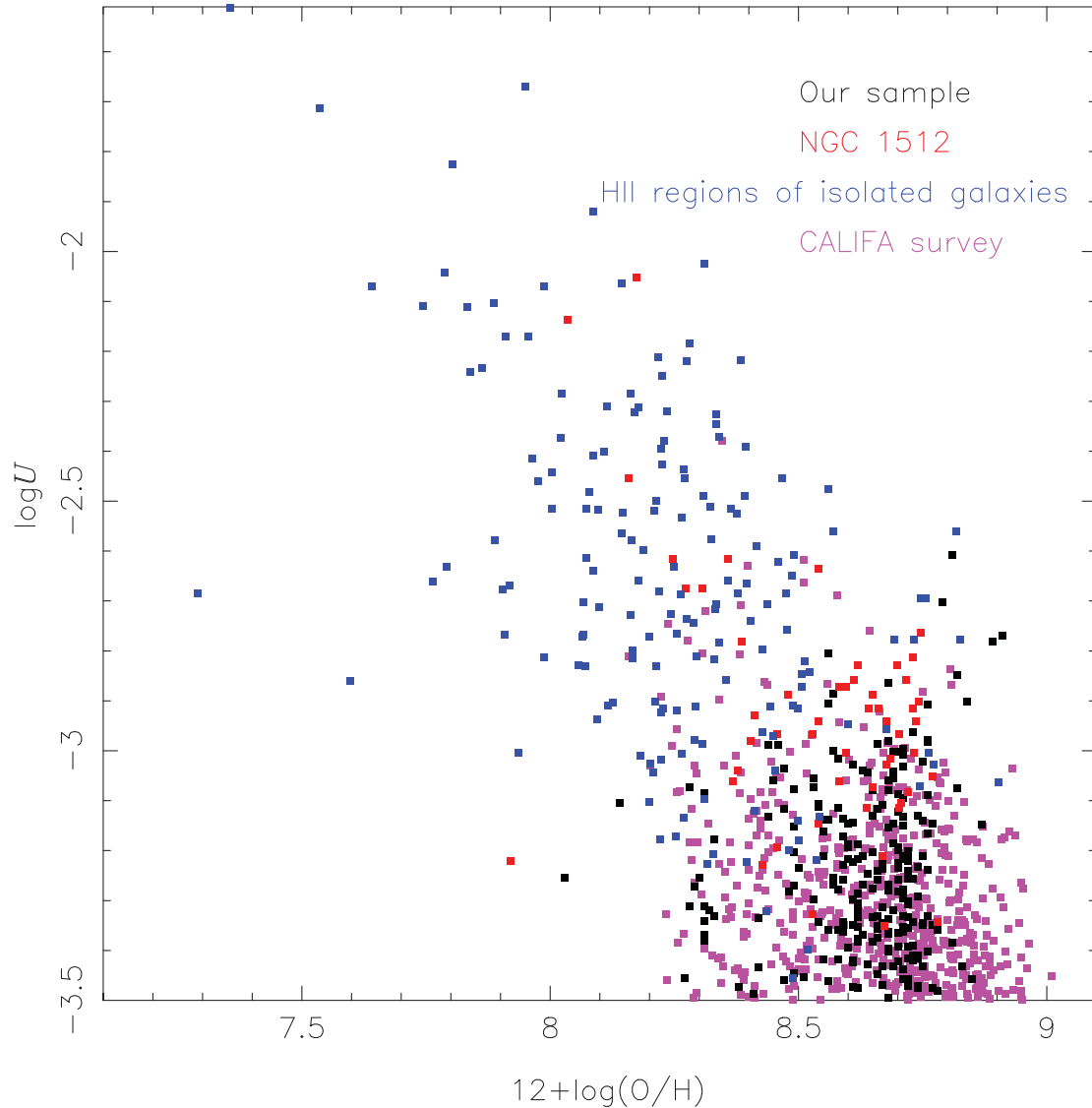
Figure 14. Ionization parameter U versus the oxygen abundances of H II regions belonging to spiral galaxies from the CALIFA survey, to isolated galaxies (data taken from Dors et al. 2011), to NGC 1512 (Bresolin et al. 2012) and from our sample, as indicated. Estimations of O/H and U were obtained using equations (1) and (4), respectively.

obtained using calibrations based on strong emission lines (N2 and O3N2). We found oxygen gradients to be significantly flatter for all galaxies in the close pairs of our sample than those found in isolated spiral galaxies. For four objects of our sample, AM 1219A, AM 1256B, AM 2030A and AM 2030B, we found a clear break in the oxygen abundance at galactocentric distances R/R_{25} of about 0.5, 0.35, 0.3 and 0.2, respectively. For two objects, AM 1219A and AM 1256B, we found negative slopes for the inner gradients, and for AM 2030B we found a positive slope. In all three cases, we found a flatter behaviour to the outskirts of the galaxies. For AM 2030A, we found a positive-slope outer gradient while the inner gradient is almost compatible with a flat behaviour. This result is not conclusive because of the small number of measured H II regions, mainly for the outer part. We found a decrease of star formation efficiency in the zone that corresponds to the oxygen abundance gradient break for AM 1219A and AM 2030B. Moreover, for AM 1219A, we also found a minimum in the estimated metallicities, indicating that this break zone could be associated with a corotation

radius. For the other two galaxies that present a gradient break, AM 1256B and AM 2030A, we found a maximum for the SFR but not an extreme oxygen abundance value. It must be noted that for all these four interacting systems, the extreme SFR values are located very close to the oxygen gradient break zones. The flattening in the oxygen abundance gradients could be interpreted as being a chemical enrichment due to induced star formation by gas flows along the discs. We have found that H II regions located in close pairs of galaxies follow the same relation between the ionization parameter and the oxygen abundance as those regions in isolated galaxies.

ACKNOWLEDGEMENTS

REFERENCES

Alloin D., Collin-Souffrin S., Joly M., Vigroux L., 1979, A&A, 78, 200
Alonso-Herrero A., Rosales-Ortega F. F., Sánchez S. F., Kennicutt R. C., Pereira-Santaella M., Díaz Á. I., 2012, MNRAS, 425, L46
Andrievsky S. M., Kovtyukh V. V., Luck R. E., Lépine J. R. D., Maciel W. J., Beletsky Yu. V., 2002, A&A, 392, 491
Andrievsky S. M., Luck R. E., Martin P., Lépine J. R. D., 2004, A&A, 413, 159
Athanassoula E., 1992, MNRAS, 259, 345
Barden M. et al., 2005, ApJ, 635, 959
Barton E. J., Geller M. J., Kenyon S. J., 2000, ApJ, 530, 660
Bastian N., Trancho G., Konstantopoulos I. S., Miller B. W., 2009, ApJ, 701, 607
Bell E. F., de Jong R. S., 2000, MNRAS, 312, 497
Bergvall N., Laurikainen E., Aalto S., 2003, A&A, 405, 31
Bernloehr K., 1993, A&A, 270, 20
Boissier S., Prantzos N., 2000, MNRAS, 312, 398
Bragaglia A., Sestito P., Villanova S., Carretta E., Randich S., Tosi M., 2008, A&A, 480, 79
Bresolin F., 2011, ApJ, 730, 129
Bresolin F., Schaerer D., González Delgado R. M., Stasińska G., 2005, A&A, 441, 981
Bresolin F., Ryan-Weber E., Kennicutt R. C., Goddard Q., 2009a, ApJ, 695, 580
Bresolin F., Gieren W., Kudritzki R.-P., Pietrzyński G., Urbaneja M. A., Carraro G., 2009b, ApJ, 700, 309
Bresolin F., Kennicutt R. C., Ryan-Weber E., 2012, ApJ, 750, 122
Cardelli J. A., Clayton G. C., Mathis J. S., 1989, ApJ, 345, 245
Castellanos M., Díaz A. I., Terlevich E., 2002, MNRAS, 329, 315
Chien L., Barnes J. E., Kewley L. J., Chambers K. C., 2007, ApJ, 660, L105
Cid Fernandes R., Mateus A., Sodré L., Stasińska G., Gomes J. M., 2005, MNRAS, 358, 363
Costa R. D. D., Uchida M. M. M., Maciel W. J., 2004, A&A, 423, 199
Dalcanton J. J., 2007, ApJ, 658, 941
Di Matteo P., Bournaud F., Martig M., 2008, A&A, 492, 31
Donzelli C. J., Pastoriza M. G., 1997, ApJS, 111, 181
Dors O. L., Copetti M. V. F., 2005, A&A, 437, 837
Dors O. L., Krabbe A. C., Hägele G. F., Pérez-Montero E., 2011, MNRAS, 415, 3616
Ellison S. L., Mendel J. T., Patton D. R., Scudder J. M., 2013, MNRAS, 435, 3627
Esteban C., Carigi L., Copetti M. V. F., García-Rojas J., Mesa-Delgado A., Castañeda H. O., Péquignot D., 2013, MNRAS, 433, 382
Ferreiro D. L., Pastoriza M. G., 2004, A&A, 428, 837
Ferreiro D. L., Pastoriza M. G., Rickes M., 2008, A&A, 481, 645
Freedman Woods D., Geller M. J., Kurtz M. J., Westra E., Fabricant D. G., Dell'Antonio I., 2010, AJ, 139, 1857
Freitas-Lemes P., Rodrigues I., Fáundez-Abans M., Dors O. L., Fernandes I. F., 2013, MNRAS, 427, 2772
Friedli D., Benz W., Kennicutt R. C., 1994, ApJ, 430, L105
Garnett D. R., Shields G. A., Skillman E. D., Sagan S. P., Dufour R. J., 1997, ApJ, 489, 63
Goddard Q. E., Bresolin F., Kennicutt R. C., Ryan-Weber E. V., Rosales-Ortega F. F., 2011, MNRAS, 412, 1246
Hägele G. F., Díaz A. I., Terlevich E., Terlevich R., Pérez-Montero E., Cardaci M. V., 2008, MNRAS, 383, 209

Hernandez-Jimenez J. A., Pastoriza M. G., Rodrigues I., Krabbe A. C., Winge C., Bonatto C., 2013, MNRAS, 435, 3342
Hummer D. G., Storey P. J., 1987, MNRAS, 224, 801
Kennicutt R. C., 1998, ARA&A, 36, 189
Kennicutt R. C., Bresolin F., Garnett D. R., 2003, ApJ, 591, 801
Kewley L. J., Ellison S. L., 2008, ApJ, 681, 1183
Kewley L. J., Rupke D., Zahid H. J., Geller M. J., Barton E. J., 2010, ApJ, 721, L48
Krabbe A. C., Pastoriza M. G., Winge C., Rodrigues I., Ferreiro D. L., 2008, MNRAS, 389, 1593
Krabbe A. C., Pastoriza M. G., Winge C., Rodrigues I., Dors O. L., Ferreiro D. L., 2011, MNRAS, 416, 38
Krabbe A. C., Rosa D. A., Dors O. L. Jr, Pastoriza M. G., Winge C., Hägele G. F., Cardaci M. V., Rodrigues I., 2014, MNRAS, 437, 1155 (Paper I)
Lambas D. G., Tissera P. B., Alonso M. S., Coldwell G., 2003, MNRAS, 346, 1189
Lemasle B. et al., 2013, A&A, 558, 31
López-Sánchez A. R., Esteban C., 2010, A&A, 516, 104
Luck R. E., Gieren W. P., Andrievsky S. M., Kovtyukh V. V., Fouqué P., Pont F., Kienzle F., 2003, A&A, 401, 939
MacArthur L. A., Courteau S., Bell E., Holtzman J. A., 2004, ApJS, 152, 175
McGaugh S. S., 1991, ApJ, 380, 140
Maciel W. J., Costa R. D. D., 2009, in Andersen J., Bland-Hawthorn J., Nordström B., eds, Proc. IAU Symp. 254, The Galaxy Disk in Cosmological Context. Cambridge Univ. Press, Cambridge, p. 38
Magrini L., Sestito P., Randich S., Galli D., 2009, A&A, 494, 95
Marino R. A. et al., 2012, ApJ, 754, 61
Marino R. A. et al., 2013, A&A, 559, 114
Martin P., Roy J. R., 1994, ApJ, 424, 599
Martin P., Roy J. R., 1995, ApJ, 445, 161
Mihos J. C., Bothun G. D., Richstone D. O., 2010, ApJ, 418, 82
Miralles-Caballero D., Díaz A. I., Rosales-Ortega F. F., Pérez-Montero E., Sánchez S. F., 2014, MNRAS, 440, 2265
Mishurov Y. N., Lépine J. R. D., Acharova I. A., 2002, ApJ, 571, L113
Mólla M., Díaz A. I., 2005, MNRAS, 358, 521
Muñoz-Mateos J. C., Gil de Paz A., Boissier S., Zamorano J., Jarrett T., Gallego J., Madore B. F., 2007, ApJ, 658, 1006
Nikolic B., Cullen H., Alexander P., 2004, MNRAS, 355, 874
Patton D. R., Ellison S. L., Simard L., McConnachie A. W., Mendel J. T., 2011, MNRAS, 412, 591
Paturel G., Garcia A. M., Fouque P., Buta R., 1991, A&A, 243, 319
Paturel G., Petit C., Prugniel P., Theureau G., Rousseau J., Brouty M., Dubois P., Cambrésy L., 2003, A&A, 412, 45
Pedicelli S. et al., 2009, A&A, 504, 81
Perez J., Michel-Dansac L., Tissera P. B., 2011, MNRAS, 417, 580
Perez M. J., Tissera P. B., Scannapieco C., Lambas D. G., de Rossi M. E., 2006, A&A, 459, 361
Pérez-Montero E., 2014, MNRAS, 441, 2663
Pérez-Montero E., Contini T., 2009, MNRAS, 398, 949
Pettini M., Pagel B. E. J., 2004, MNRAS, 348, L59
Pilyugin L. S., 2003, A&A, 397, 109
Pilyugin L. S., Thuan T. X., 2005, ApJ, 631, 231
Pilyugin L. S., Grebel E. K., Mattsson L., 2012, MNRAS, 424, 2316
Pohlen M., Trujillo I., 2006, A&A, 454, 759
Portinari L., Chiosi C., 1999, A&A, 350, 827
Rodríguez-Baras M., Rosales-Ortega F. F., Díaz A. I., Sánchez S. F., Pasquali A., 2014, MNRAS, 442, 495
Rosales-Ortega F. F., Díaz A. I., Kennicutt R. C., Sánchez S. F., 2011, MNRAS, 415, 2439
Rupke D. S. N., Kewley L. J., Barnes J. E., 2010a, ApJ, 710, L156
Rupke D. S. N., Kewley L. J., Chien L.-H., 2010b, ApJ, 723, 1255
Sánchez S. F. et al., 2012, A&A, 546, 2
Sánchez S. F. et al., 2014, A&A, 563, 49
Scarano S., Lépine J. R. D., 2013, MNRAS, 428, 625
Scarano S., Lépine J. R. D., Marcon-Uchida M. M., 2011, MNRAS, 412, 1741

Scudder J. M., Ellison S. L., Torrey P., Patton D. R., Mendel J. T., 2012, MNRAS, 426, 549

Shaver P. A., McGee R. X., Newton L. M., Danks A. C., Pottasch S. R., 1983, MNRAS, 204, 53

Stasińska G., 2006, A&A, 454, L127

Storchi-Bergmann T., Calzetti D., Kinney A. L., 1994, ApJ, 429, 572

Toomre A., Toomre J., 1972, ApJ, 178, 623

Torres-Flores S., Scarano S., Mendes de Oliveira C., de Mello D. F., Amram P., Plana H., 2014, MNRAS, 438, 1894

Trancho G., Bastian N., Miller B. W., Schweizer F., 2007, ApJ, 664, 284

Trujillo I. et al., 2004, ApJ, 604, 521

Vílchez J. M., Esteban C., 1996, MNRAS, 280, 720

Werk J. K., Putman M. E., Meurer G. R., Santiago-Figueroa N., 2011, ApJ, 735, 71

Wright E. L., 2006, PASP, 118, 1711

Yong D., Carney B. W., Friel E. D., 2014, AJ, 144, 95

Zahid H. J., Bresolin F., 2011, AJ, 141, 192

Zaritsky D., Kennicutt R. C., Huchra J. P., 1994, ApJ, 420, 87

SUPPORTING INFORMATION

Additional Supporting Information may be found in the online version of this article:

Table 3. Specific parameters and intensity of emission lines corrected by reddening (relative to Hβ = 100) (http://mnras.oxfordjournals.org/lookup/suppl/doi:10.1093/mnras/stu1578/-/DC1).

Please note: Oxford University Press is not responsible for the content or functionality of any supporting materials supplied by the authors. Any queries (other than missing material) should be directed to the corresponding author for the article.

This paper has been typeset from a TEX/LATEX file prepared by the author.